

## DEFORMATION OF FOOD POWDERS BY NANOINDENTATION

Y.A. Yusof<sup>1</sup>, A.C. Smith<sup>2</sup>, and B.J. Briscoe<sup>3</sup>,

<sup>1</sup>Department of Process and Food Engineering,

Faculty of Engineering, Universiti Putra Malaysia, 43400, Serdang, Selangor, Malaysia.

<sup>2</sup>Institute of Food Research, Norwich Research Park, Colney, Norwich NR4 7UA, UK.

<sup>3</sup>Department of Chemical Engineering & Chemical Technology,

Imperial College London, London SW7 2AZ, UK.

Email: [niza@eng.upm.edu.my](mailto:niza@eng.upm.edu.my)

### ABSTRACT

*Nanoindentation is a test where an indenter induces a localised deformation into a sample surface to determine its material properties, such as hardness and modulus of elasticity, at nanometre scale. The depth indentation technique was used in this study. The technique is based on the recording of the applied force as a function of penetration depth during the loading and unloading processes. In this paper, the compacted fine maize, coarse maize, and Avicel were investigated upon nanoindentation. The test was conducted so that the deformability of the food powders, which behave as viscoelastic materials, may be understood better. It was found that Avicel powder forms a stronger and more coherent junction compared to maize powders, as evidenced from their measured hardness and modulus of elasticity.*

**Keywords:** nanoindentation, food powders, deformation, force, loading-unloading processes, viscoelastic

### INTRODUCTION

There have been many approaches to studying the mechanical behaviour of powder materials. Amongst the first was the imaging technique to measure the material hardness. However, this technique requires an optical or mechanical evaluation of the contact cross-sectional area commonly associated with large and unacceptable errors, particularly for a very shallow nanometre-scale indent. Of more conventional is the uniaxial die compaction technique, which measures the bulk deformation of the material upon loading force. This technique however is not suitable for soft and thin materials.

Since the 1980s many researchers have adapted the measurements of mechanical properties by indenting a sharp and rigid probe into a very thin surface layer of the materials [1, 2, 3, 4]. So-called contact compliance method, it is based upon the investigation of the force-displacement curve obtained from loading and unloading of the indentation process, and is capable of characterising correctly – e.g. using indentation forces ranging from 100  $\mu\text{N}$  to 10 mN [5] – the surface molecular layers. When applied at nanometre scale, the method is called nanoindentation technique. This method is very useful to characterise polymeric [4, 6, 7, 8] and food materials [9], thus providing the basic data required for design purposes and quality assessment.

#### Force-displacement Curve

In this paper, the values of hardness and modulus of elasticity of food powders were calculated by adopting force-displacement curves. Figure 1 shows two curves in the indentation force-displacement diagram: the loading curve OB describes the gradual increase of the displacement  $h$  as the force  $P$  is gradually applied, and the unloading curve BC describes the gradual decrease of the displacement as the force is gradually removed. The maximum displacement  $h_{max}$  corresponds to the maximum force  $P_{max}$ , and the final displacement  $h_f$ , called the residual displacement, corresponds to the complete unloading. The unloading curve is particularly useful in the description of material behaviour. The line BD tangent to the curve at the maximum displacement represents the elastic deformation [1, 3, 7, 11], the line BC represents the viscoelastic behaviour, and the line BG represents the plastic behaviour [2]. Note that, upon unloading (or complete removal) of the applied force, the elastic material returns to its original size and shape, plastic material deforms permanently, and viscoelastic material deforms in a manner that is intermediate between the two formers [10].

The material hardness could be obtained via the contact stiffness  $S^*$ . This is represented by the slope of line BD, and is formulated in relation to the apparent displacement  $h_e$  (i.e. the intercept of the tangent line BD) as:



$$P = \alpha_I (h - h_f)^{m_I} \quad (5)$$

where  $\alpha_I$  is the geometric constants of the material elastic modulus and  $m_I$  is the power law exponent that is related to the geometry of the indenter ( $m_I = 1$  for a flat-ended cylindrical punch,  $m_I = 1.5$  for a paraboloid of revolution, and  $m_I = 2$  for a cone).

An alternative expression for the contact stiffness is that of Pharr et al.[19]:

$$S = 2a_I E_r = \frac{2\beta}{\sqrt{\pi}} E_r \sqrt{A_I} \quad (6)$$

where  $a_I$  is the contact radius,  $E_r$  is the reduced modulus due to the deformations of the indenter and the material,  $A_I$  is the projection of the contact area of the tip-material contact, and  $\beta$  is a parameter which varies slightly with the indenter geometry ( $\beta = 1$  for a circular indent cross section,  $\beta = 1.034$  for a triangular indent cross section, and  $\beta = 1.012$  for a square indent cross section). The reduced modulus  $E_r$  is written as:

$$\frac{1}{E_r} = \frac{(1 - \nu_p^2)}{E} + \frac{(1 - \nu_{pI}^2)}{E_I} \quad (7)$$

where  $E$  and  $\nu_p$  are respectively the modulus of elasticity and the Poisson's ratio of the material, and  $E_I$  and  $\nu_{pI}$  are those of the indenter.

The stiffness could also be obtained from the hardness of the material from the conical and pyramidal indenter is:

$$H_d(h_c) = \frac{P_{\max}}{A_I} = \frac{P_{\max}}{ch^2} \quad (8)$$

where  $c$  is a constant that depends upon the indenter geometry.

Correlating the stiffness is defined by the slope of the tangent line of the unloading curve at the maximum loading point ( $h_{\max}, P_{\max}$ ) and is given as [3]:

$$S^* = \left( \frac{dP}{dH_d} \right)_{(h_{\max}, P_{\max})} = \alpha_I m_I (h_{\max} - h_f)^{m_I - 1} \quad (9)$$

When  $S^* = S$ , the tangent line describes an unloading path at a constant contact area with  $h_c = h_{\max} - h_s$ . Oliver and Pharr [3] have introduced  $h_s$  as:

$$h_s = \frac{\varepsilon_I P_{\max}}{S} \quad (10)$$

where  $h_s$  is defined as the elastic displacement of the surface at the contact parameter that depends upon the tip shapes and  $\varepsilon_I$  is a function of the tip geometry. Due to the viscoelastic behaviour of the material, the modulus of elasticity depends upon time and the hydrostatic pressure [5]. The viscoelastic recovery can be presented as  $h_c - h_f$ , which is the immediate elastic depth recovery [5]. For a flat-ended cylindrical punch  $\varepsilon_I = 1$ , for a paraboloid of revolution  $\varepsilon_I = 0.75$ , and for a cone  $\varepsilon_I = 2(\pi - 2)/\pi$ . Therefore,  $h_c$  is given as:

$$h_c = h_{\max} - \frac{\varepsilon_I P_{\max}}{S} \quad (11)$$

#### Calibration for the Nanoindentation Test

The experimental procedure of the nanoindentation test involves two types of calibrations, the force compliance  $C_f$  and tip shape area function  $A_I(h_c)$  [5]. An iterative technique may be used to calculate those calibrations.

### Force-frame Compliance Calibration

For the force-frame compliance calibration, the total displacement  $h_{total}$  is obtained by treating the system as two-springs (the force frame and the material) and is given as:

$$h_{total} = h_{ff} + h_{samp} \quad (12)$$

where  $h_{ff}$  is the displacement of the force frame and  $h_{samp}$  is the displacement of the material. Then, the total compliance is given as:

$$C_{total} = C_{ff} + C_s = C_{ff} + \frac{\sqrt{\pi}}{2E_r} \frac{l}{\sqrt{A_I}} \quad (13)$$

where the total compliance is  $C_{total}=1/S^*$  and the material compliance is  $C_s=1/S$ . In order to determine the value of  $C_{ff}$ , a series of indentation measurements are made on a reference material, for instance fused silica. Large indentation forces and displacements are applied to the reference material to exhibit large plastic deformation and contact stiffness  $S^*$ . Consequently, total compliance  $C_{total}$  will be dominated by the force, arising from frame compliance  $C_{ff}$ .

### Tip Shape Area Calibration

Another calibration involved for the nanoindentation test is the tip shape area calibration. A series of indentations are applied to the reference material for a range of maximum force and displacement to measure the cross-sectional area of the indenter tip as a function of distance from the apex. The projection of the contact area  $A_I$  is written as a function of the actual contact displacement  $h_c$  as:

$$A_I(h_c) = ch_c^2 \quad (14)$$

where  $A_I$  is the cross-sectional area of the indenter tip at a distance  $h_c$  (contact displacement), which is related to the contact radius  $a_I$ . By fitting the tip shape function to a multi-term polynomial:

$$A_I(h_c) = B_0 h_c^2 + B_1 h_c + B_2 h_c^{1/2} + B_3 h_c^{1/4} + B_4 h_c^{1/8} \dots \quad (15)$$

where  $B_0, B_1, \dots, B_n$  are the constant coefficients from the curve fitting. By considering the tip imperfections, Oliver and Pharr [3] have suggested to use the contact area function  $A_I(h_c)$  up to 9 terms ( $n=8$ ) of the polynomial equation with  $B_0=24.5$ . For a Berkovich indenter, the contact area function is [3].

$$A_I(h_c) = 24.5h_c^2 \quad (16)$$

### Calculation of Hardness and Modulus of Elasticity Values

After the calibration of both the force frame compliance and the tip shape area function, measurements of the force-displacement (see Fig. 1) of the material can be conducted.

Firstly the unloading curve is fitted to equation (5), and the fitting parameter  $m_I$  is used to calculate the contact stiffness  $S^*$  in equation (9), which is equal to the stiffness  $S$  by assuming that the force compliance  $C_{ff}$  value is correct. Then, the intercepting line  $h_c$  is calculated using equation (11) and is used to calculate the contact area  $A_I$  using equation (16). Therefore, the value of the modulus of elasticity  $E$  can be calculated using equation (7), by calculating the reduced modulus  $E_r$  in equation (6). The value of hardness may simply be obtained from equation (8).

### Errors from the Compliance Method

There are several factors affecting the indentation measurements. These are the initial displacement, the shape of the indenter tip, the shape of the impression (pile-up and sink-in), the surface roughness, the machine compliance, the thermal drift, errors in the force-displacement measurement, noise and the after-effects in the system upon unloading, the elasticity of the indenter, and the homogeneity of the material properties [20].

Briscoe et al. [5] mentioned that during the calibration process against a hard surface, such as the fused silica, an additional error may be induced due to a Hertzian like deformations of the indenter tip, particularly at the beginning of the contact. However, this effect may not represent a similar contact situation for softer material such as polymers. Hertzian contact means an elastic contact of a single spherical solid [21].

Problems, such as indenter tip imperfections, may occur at the smallest displacement during the indentation experiments, particularly when sharp points (pyramidal or cone shaped) are used [4, 7, 8]. This defect may cause significant errors in the hardness evaluation. Briscoe and Sebastian [4] introduced an analytical procedure to solve this problem in polymeric material by estimating the tip defect, thus reducing the error source.

Polymeric material, including food materials, exhibit viscoelastic deformation [5]. Such deformation may provide the values of hardness and the modulus of elasticity that depend upon the geometry of the displacement, the displacement (strain), the loading rate (strain rate), and the ambient temperature [5]. Reducing the displacement, the value of modulus of elasticity causes the hardness to increase; this effect is called an indentation size effect (ISE), which is particularly notable for displacement less than 100 nm [22]. This may be caused by friction, lack of measurement capabilities, surface layers, oxides, and chemical contamination [23], and nonuniform deformation of the material [23, 24]. The most likely cause is the tip defect where the normally sharp tip becomes blunt and rounded.

Viscoelastic creep may also occur to the material [2, 5]. It may increase the initial slope of the unloading and affect the stiffness value, consequently the evaluation of the modulus of elasticity. To reduce this effect, Briscoe et al. [5] have suggested that a 10 s 'hold' period is introduced during the unloading.

Surface roughness effects are caused by the asperities that exist on the material surfaces, and it is recommended to ignore the values of hardness and modulus of elasticity at the displacement lower than 20 to 50 nm [20]. The shape of the impression may also affect the contact area of an indent, causing pile-up and sink-in effects, which may cause the material to be displaced to the side of the indenter during the indentation [25]. The pile-up of the material results in a contact area larger than the cross-sectional area of the indenter at the apparent displacement. Whereas the sink-in effect results in an apparent displacement, which is smaller than the cross-sectional area of the indenter used, and are caused by the elastic displacement of the material.

Other than that, there is the thermal effect (Joule effect) during the indentation experiment. Temperature changes occur to the material due to fluctuations of the environment temperature and Joule heating in the force application coil [5]. However, this effect is only significant for experiments conducted over a long period of time [3, 20].

## **MATERIALS AND METHODS**

### **Materials**

The deformability of fine and coarse maize, and Avicel powders upon nanoindentation were investigated and described below. The nanoindentation measurement of each of the sample was performed in the Department of Chemical Engineering and Chemical Technology, Imperial College London, UK.

### **Avicel**

Microcrystalline cellulose, trade name Avicel PH 102, is manufactured by FMC, USA and in this paper it is referred to as Avicel with the mean particle size of 80  $\mu\text{m}$ . It is purified, partially depolymerised cellulose that is white, tasteless, odourless, and having a crystalline structure composed from porous particles [26]. Avicel is commonly used as a filler-binder due to its excellent bonding properties, allowing plastic deformation to occur. It has been widely used as excipient in dry and wet granulation in pharmaceutical processing.

### **Maize**

Maize has been recognised as one of the major sources of food for a large number of people, particularly in developing countries. For instance, in Mexico, maize is very popular for cooking tortillas, the well-known Mexican bread. Maize may provide a significant amount of nutrient in terms of carbohydrate (calories) and protein.

There are two sizes of maize powder used. The fine maize (Fine Polenta F) with the mean particle size of 135  $\mu\text{m}$  and coarse maize, which is the maize grits, with the mean particle size of 632  $\mu\text{m}$  [12]. Both the maize powder and the maize grits were yellow in colour, and were obtained by dry milling, from F. Smiths Mills Worksop, UK. The dry matter composition of the maize was 80.5% starch (carbohydrate), 13% protein, 1.7% dietary fibre, 1.4% fat, 0.7% free sugar and 0.2% ash. Note that, the composition for both maize powder and maize grits were similar.

### Preparation of Materials

As the particle sizes of the powder used were relatively small, preliminary compaction using EZ-50 Materials Testing Machine (Llyods Instruments Ltd., UK) were carried out. The powders were prepared in the form of compacts using a 20 mm-cylindrical stainless steel die by applying pressure of 127 MPa each. Hence, the densities of the compacts were assumed approaching to the values of the true density of the powders, respectively. Therefore, the porosities of the powder may be neglected and each of the compacts may be treated as a particle. The procedure to prepare the compacts was similar to that used for the uniaxial die compaction [14].

### Nanoindentation

A NANO INDENTER®II (Nano Instruments Inc. Tennessee, USA) is a machine used to measure hardness and modulus of elasticity of materials by applying forces in the microgram range. It is based upon force-controlled and displacement-controlled systems, which can be measured continuously as a function of indenter displacement (see Figure 2 and 3). The major parts of this machine are:

- 1) An indenter
- 2) An optical microscope
- 3) A precision table that support the microscope and the indenter.

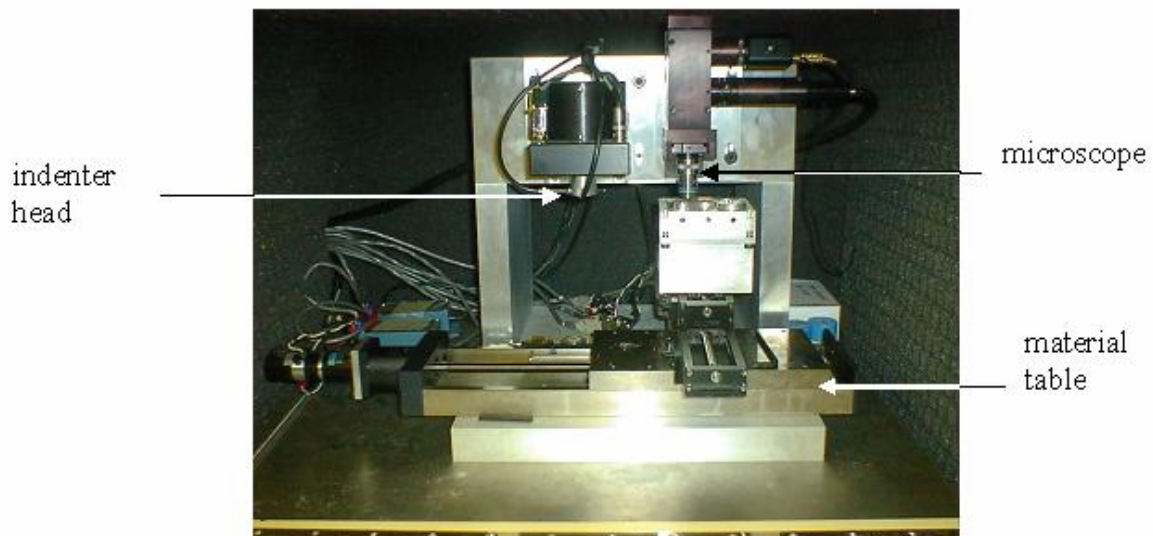


Figure 2: The nanoindenter

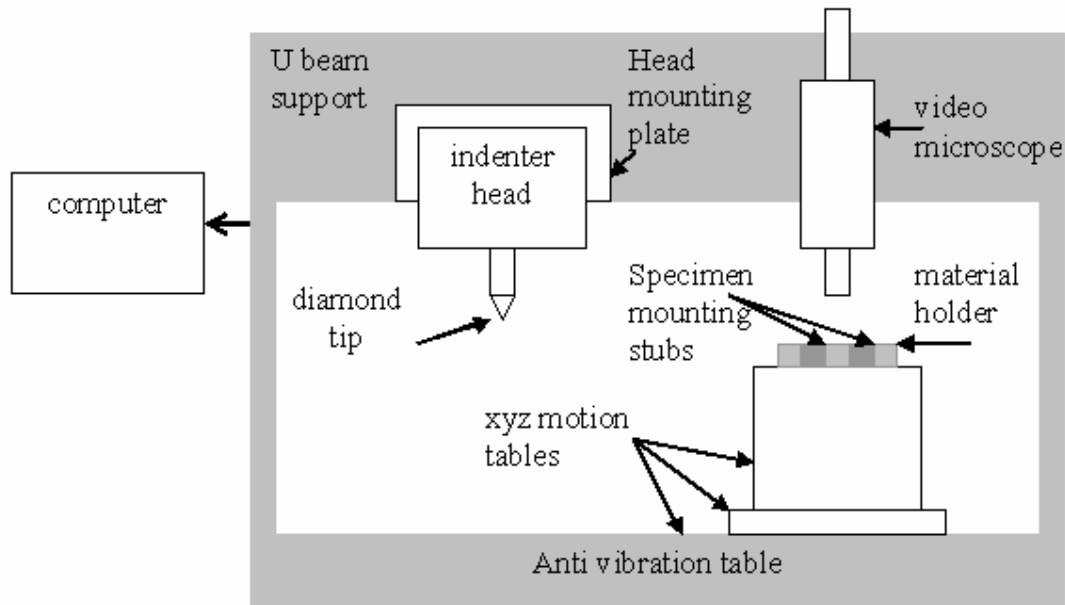


Figure 3: The nanoindentation system

### Experimental Procedures for Nanoindentation

There are two segments used during the indentation - loading and unloading. The loading segment, also known as the 'approach' segment, will accurately determine the 'zero' effect of the indent, that is the value of the indenter force and displacement at the initial position where the tip touches the surface of the material.

First, the compact was glued to a standard metallographic mount by using the epoxy resin, and tightened to the material holder by the Allen screw. An area for the indentation was selected by using an optical location system at 80 times magnification. Then, the material was moved by the  $x$ - $y$  table from beneath the microscope, to a point beneath the indenter. The  $z$ -stage moved the material up for first surface finding indent, and backs the material away to a distance half of the offset. Again, the  $z$ -stage moved the material up for the second finding indent. At this stage the indenter was left in contact with the surface under a very small force, and the system monitored the changes in displacement  $h$  under constant force and calculated the drift rate  $dh/dt$ . The displacement of the indenter was recorded and an initial estimate of the elevation of the material surface was established. The drift rate was monitored for three consecutive readings to ensure that the values were lower than the user-prescribed, maximum defaults of  $0.05 \text{ nms}^{-1}$ . Then the indenter was moved up using the coil-magnet assembly while the table remained fixed until the next surface was found. Finally the material was moved to the first surface indent and the experiment started by lowering the indenter into the surface at the approach rate of  $10 \text{ nms}^{-1}$ , above the estimated elevation of the material surface. A force-displacement curve generated from the indentation was recorded. The 'approach' segment was considered complete when the stiffness of the material had increased to a factor of 4. The zero point was taken from the average of both the force and displacements of 12<sup>th</sup> and 13<sup>th</sup> data point (3000 nm) at the end of the approach data. After determining the surface contact, the second segment, the unloading, was carried out by moving the indenter up from the surface. The stiffness of the sample was calculated from the unloading curve by using a compliance method adopted by Oliver and Pharr [3].

For the next indentation, the surface contact determined earlier was used for other indents. In this study, about 10 indentations were carried out for each compact and a continuous stiffness type of measurement was applied. The continuous stiffness measurement was the measurement of the material hardness and modulus of elasticity of the material during the entire loading segment.

### Tip Calibration

For tip calibration a Berkovich indenter was used to indent the fused silica at approximately  $5 \mu\text{m}$ . Note that, the area function was assumed a reference material, corresponded to the perfect pyramid shape of the indenter. A variation of displacements was applied and results in a series of measurements, which were used to fit equation (15). The constant coefficients of the fitting for the current system are  $B_1 = 254.71$ ,  $B_2 = 3.860 \times 10^{-5}$ ,  $B_3 = 7.947$

$\times 10^{-4}$ ,  $B_4 = 9.226 \times 10^{-4}$ ,  $B_5 = 2.2787 \times 10^{-3}$ ,  $B_6 = 16.39$ ,  $B_7 = 31.06$ , and  $B_8 = 1.4213$ . Then, the value of modulus of elasticity of fused silica was evaluated by using equation (6) and (7) at the largest displacement

## RESULTS AND DISCUSSION

### Loading and Unloading Curves

Figure 4 shows the loading and unloading curves of compacted fine maize, coarse maize, and Avicel powders upon the displacement of the indenter, with a strain rate of  $0.1 \text{ s}^{-1}$ . Avicel, which was quite shallowly indented compared to fine maize and coarse maize, shows a pronounced recovery of elastic work. This behaviour agrees well with the Avicel characteristics in the microscopic study [12]. It was also observed that the loading curve shows a smooth curve which may be used to indicate that Avicel powder flows plastically and has a ductile characteristic; thus, producing a strong and coherent compact. Note that, if the loading curve is discontinuous, or so-called “pop-in-points” occur, the material may be characterised as having a brittle characteristic [14]. The general trend of the results obtained for nanoindentation of Avicel compact was found similar to those of Mohammed [15], which was compacted at the pressure of 246 MPa. However, the maximum contact displacement applied by Mohammed [15] was very shallow at approximately 1200 nm ( $1.2 \mu\text{m}$ ), and prior to indentation, a ‘hold’ segment was added for 60 seconds to reduce the creep effect. In this study, the hold segment is not introduced; however, in order to reduce the creep effect, the compact was indented at a deeper displacement (penetration depth), and hence, higher force, many times of Mohammed’s [15]. This method was applied based upon the findings of Briscoe et al. [5] that, at low force, the hardness analysis depend upon the hardness of the material and vice versa. Creep is defined as the decrease of displacement under a constant force. It is usually noticed as having a rather peculiar round shape of data at the peak of the loading and unloading curves, or the presence of a ‘nose’ [5].

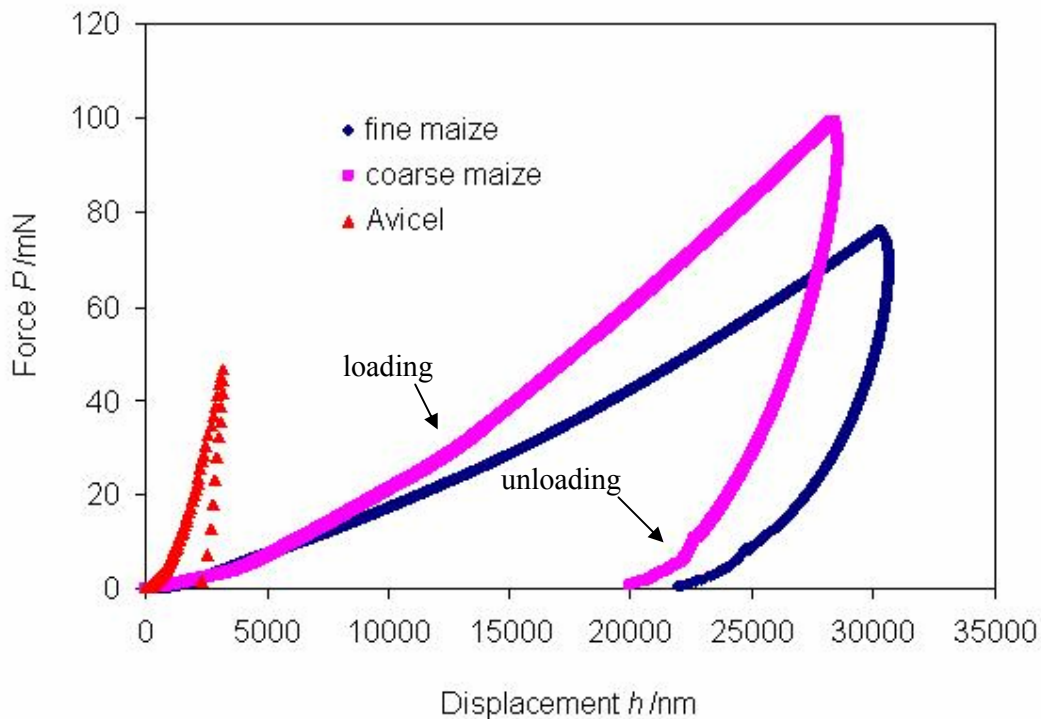


Figure 4: Loading and unloading curves of powders from nanoindentation

In Figure 4 both the fine maize and coarse maize show smooth loading curves, which may indicate that the maize powder’s intrinsic properties are slightly ductile. However, upon unloading, both of the curves show a large amount of stored elastic strain, or high elastic recovery, hence more energy was dissipated, and consequently it was difficult for the maize powder to be formed into a strong and coherent compact. As the main surface composition of the maize powder contains starch, this study may be compared to the results obtained by Mohammed [15] for nanoindentation of a pure starch. The loading curve for the starch was also smooth, and had a large amount of elastic recovery [15]. However, the extent of the elastic recovery was considered by Mohammed [15] as a two-fold matter; therefore, a higher extent of elastic recovery does not mean that a

material may form a strong and coherent junction strength, like those found for starch and Avicel powders [15]. Junction strength is the strength of the inter-particle contact. Further evidence to support these findings is given in the next section.

### Hardness and Modulus of Elasticity

Figure 5 shows the values of hardness of fine maize, coarse maize, and Avicel powders as a function of displacement with the strain rates maintained constant at  $0.1 \text{ s}^{-1}$ . The value of hardness was obtained by calibrating the force frame compliance and the tip shape area function [5]. The indenter tip was assumed as perfectly sharp, an ideal Berkovich pyramid, and a series of indentations were made with fused silica as the reference material. Then, the projection of the contact area  $A_I$  was calculated by using equations (14) and (16), consequently, the value of hardness was calculated using equation (8).

Table 1: Values of hardness and modulus of elasticity of powders

Powder	Hardness $H_d$ /MPa	Modulus of Elasticity $E$ /MPa
Fine maize	$5.6 \pm 2.9$	$128.9 \pm 43.8$
Coarse maize	$13.3 \pm 7.6$	$249.7 \pm 142.1$
Avicel	$230.3 \pm 65.3$	$435.5 \pm 105.0$

Figure 6 shows the values of modulus of elasticity as a function of displacement for fine maize, coarse maize, and Avicel powders, with the strain rates maintained constant at  $0.1 \text{ s}^{-1}$ . The value of modulus of elasticity was calculated by using equations (6) and (7); with the modulus of elasticity, and the Poisson's ratio of the diamond tip of the indenter was taken as 1141 GPa and 0.07, respectively [3], and the Poisson's ratio of fine maize, coarse maize, and Avicel powders were 0.30, 0.32, and 0.28, respectively, estimated based upon Muller's [27] data. Note also that the data in Figure 6 and 7 were averaged from 7 to 10 experiments; however, for clarity, error bars are not shown.

Both Figures 5 and 6 show that the values of hardness and modulus of elasticity decrease as the displacement increases and becomes constant at 2500 nm ( $2.5 \mu\text{m}$ ) and above for all of the powders used. Note that those parts of compacts that are close to the surface are harder and this resulted in higher values of hardness and modulus of elasticity. A similar trend was obtained by Briscoe et al. [5] for a microscopic study and by Briscoe and Sebastian [4] for a macroscopic study upon polymeric materials. This may be called as an indentation size effect (ISE), particularly at a penetration depth less than 100 nm [20, 22]. The main cause of this problem may be due to the tip defect - the nominally sharp tip becomes blunt and rounded. Other causes are due to the decrease of signal-to-noise ratios at low load and displacement levels [22]. Furthermore, as elucidated earlier, the powders tested in this study were in the form of compacts; therefore, it is expected that the values of hardness and modulus of elasticity greatly depend upon the density distribution of the powders in the compact. In conjunction with the level of the displacement, the density distribution is not uniform, or, in other words is inhomogeneous. This problem is more significant at the near-to-surface area of the compact, which has been demonstrated by Train [28] for the density distribution of a compact using a lead-shot method. It is also important to realise that the compacts, which are usually composed of particles and pores, may not be used to reflect the deformation of the powders as a particle.

In order to avoid the ISE effect, the displacement (penetration depth) of the indenter was carried out deeper, which was between 3000 to 20 000 nm (3 to 20  $\mu\text{m}$ ) more than those usually being used in the literature of between 1200 nm (1.2  $\mu\text{m}$ ) for pharmaceutical material [15] to 10 000 nm (10  $\mu\text{m}$ ) for polymeric material [5]. The data of hardness and modulus of elasticity given in Table 1 were averaged out after the maximum contact displacement of 2500 nm ( $2.5 \mu\text{m}$ ).

In Table 1, Avicel has the highest value of hardness and modulus of elasticity compared to both of the maize powders. This agrees well with Roberts and Rowe [29] that starch (one of the maize components) and Avicel have the same yield pressure but their values of hardness and modulus of elasticity are different. Comparing the data calculated in Table 1 with the values obtained from the macroscopic study from Roberts and Rowe [29], the values of  $E$  for starch (one of the maize components) and Avicel powders are 2 to 5 GPa (2000 to 5000 MPa) and 5 to 15 GPa (5000 to 15000 MPa), respectively; whereas the values of  $H$  for starch and Avicel powders are 0.05 to 0.15 GPa (50 to 150 MPa) and 0.16 to 0.60 GPa (160 to 600 MPa), respectively. Roberts and Rowe [29] indented these materials using microindentation with spherical and pyramidal indenters. The values of modulus of elasticity and hardness of Avicel powder from this study are comparable with those found in the literature, whereas the values of modulus of elasticity and hardness of maize powders obtained from this study are ten times less than those found from the literature. However, these findings may be supported by VanLandingham

et al. [22] in that the microindentation values are usually higher than that obtained from the nanoindentation. In addition, other factors which have significant effects on food materials, such as time, temperature, and moisture, may have also caused the deviation of the values of modulus of elasticity.

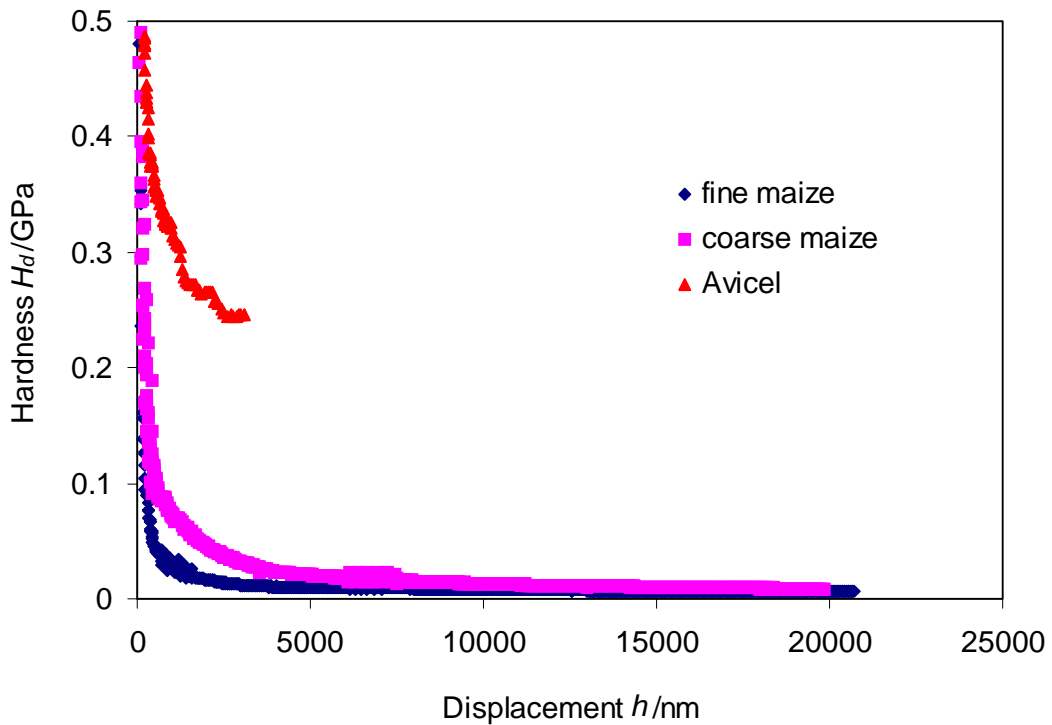


Figure 5: Hardness as a function of displacement from nanoindentation with the strain rate of  $0.1 \text{ s}^{-1}$

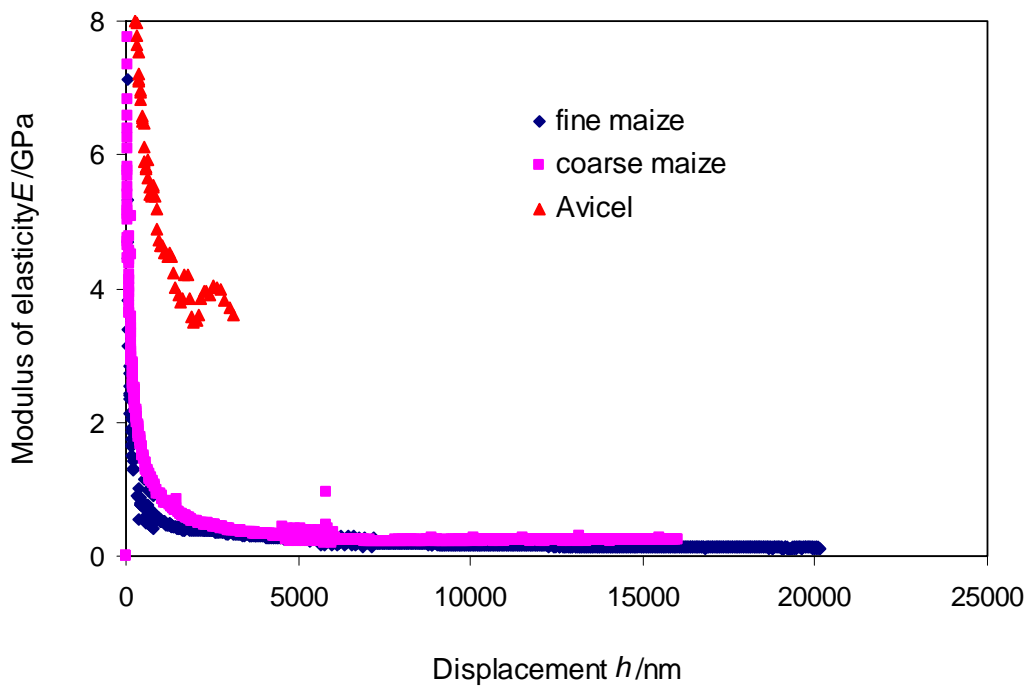


Figure 6: Modulus of elasticity as a function of displacement from nanoindentation with the strain rate of  $0.1 \text{ s}^{-1}$

## CONCLUSIONS

From the loading and unloading curves of compacted fine maize, coarse maize, and Avicel powders, it was found that, during loading, maize powders were slightly ductile and, upon unloading, both of the powders had stored a large amount of elastic strain, and consequently, were more difficult to form into a strong and coherent compact. Even though Avicel showed the same behaviour, it was able to form strong and coherent junctions. These differences may be explained by inferring that the strength of the starch junctions in the maize powder was relatively low compared to the crystalline junction formed by the Avicel powder. The values for hardness of fine maize, coarse maize, and Avicel powders are 0.01, 0.01, and 0.23 GPa, respectively. While, the values of the modulus of elasticity of fine maize, coarse maize, and Avicel powders are 0.13, 0.25, and 4.35 GPa, respectively. In conclusion, the use of the indentation technique to investigate the viscoelastic nature of food materials is expected to have wide application in the future.

## ACKNOWLEDGEMENTS

The authors would like to acknowledge Mr. Dan Parsonage, Imperial College London for technical assistance. One of the authors (Y.A.Y.) is also grateful for the scholarship from Universiti Putra Malaysia, Malaysia and A.C.S. was funded from the BBSRC competitive strategic grant.

## REFERENCES

- [1] Pethica, J.B., Hutchings, R. and Oliver, W.C. (1983) Hardness measurement at penetration depths as small as 20 nm. *Philosophical Magazine A*. **48**(4): 593-606.
- [2] Doerner M.F. and Nix W.D. (1986) A method of interpreting the data from depth-sensing indentation instruments. *Journal of Materials Research* **1**(4): 601-609.
- [3] Oliver W.C. and Pharr G.M. (1992) An improved technique for determining hardness and elastic modulus using load and displacement sensing indentation experiments. *Journal of Materials Research* **7**(6): 1564-1583.
- [4] Briscoe, B.J. and Sebastian, K.S. (1996) The elastoplastic response of poly(methyl methacrylate) to indentation. *Proceedings of the Royal Society London A* **452**: 439-457.
- [5] Briscoe B.J., Fiori L. and Pelillo E. (1998) Nano-indentation of polymeric surfaces. *Journal of Physics D: Applied Physics* **31**: 2395-2405.
- [6] Ion, R.H., Pollock, H.M. and Roques-Carnes, C. (1990) Micron-scale indentation of amorphous and drawn PET surfaces. *Journal of Materials Science* **25**: 1444-1454.
- [7] Briscoe B.J., Sebastian K.S. and Adams, M.J. (1994) The effect of indenter geometry on the elastic response to indentation. *Journal of Physics D: Applied Physics* **27**: 1-7.
- [8] Briscoe B.J., Sebastian K.S. and Sinha S.K. (1996) Application of the compliance method to the microhardness measurement of organic polymers. *Philosophical Magazine A*. **74**(5): 1159-1169.
- [9] Özkan, N., Xin, H. and Xiao, D.C. (2002) Indentation test examination. *Science Report NZ* : 23-26.
- [10] Ward, I.M. (1983) *Mechanical Properties of Solid Polymers*, 2<sup>nd</sup> Edition, John Wiley & Sons, England.
- [11] Loubet, J.L., George, J.M., Marchesini, O. and Meille, G. (1984) Vickers indentation curves of MgO. *Transaction of the ASME: Journal of Tribology* **106**: 43-48.
- [12] Yusof, Y.A. (2005) Rolling-mill granulation of powders. D.Phil Thesis, Department of Chemical Engineering and Chemical Technology, Imperial College London, United Kingdom.
- [13] Yusof, Y.A., Smith, A.C. and Briscoe, B.J. (2005) Roll compaction of maize powder. *Chemical Engineering Science* **60**(14): 3919-3931.
- [14] Adams, M.J., Akram, A., Briscoe, B.J., Lawrence, C.J. and Parsonage, D. (1999) Nanoindentation of particulate coatings. *Journal of Materials Research* **14**(6): 2344-2350
- [15] Mohammed, H. (2004) Contact Mechanical Aspects of Pharmaceutical Compaction. D.Phil Thesis, Department of Chemical Engineering and Chemical Technology, Imperial College London, United Kingdom.
- [16] Oliver W.C., Hutchings, R. and Pethica, J.B. (1986) An improved technique for determining hardness and elastic modulus using load and displacement sensing indentation experiments. *Journal of Materials Research* **7**(6): 1564-1583.
- [17] Box, G.E.P. and Cox, D.R. (1964) An analysis of transformations. *Journal of the Royal Statistical Society* **26**: 211-243.
- [18] Sneddon, I.N. (1965) The relation between load and penetration in the axisymmetric boussinesq problem for a punch of arbitrary profile. *International Journal of Engineering Science* **3**: 47-57.

- [19] Pharr, G.M., Oliver, W.C. and Brotzen, F.R. (1992) On the Generality of the Relationship Among Contact Stiffness, Contact Area, and Elastic Modulus During Indentation. *Journal of Materials Research* **7**: 613-617.
- [20] Menčík, J. and Swain, M.V. (1995) Errors associated with depth-sensing microindentation tests. *Journal of Materials Research* **10**(6): 1491-1501.
- [21] Hertz, H. (1895) On the contact of elastic solids. In *Hertz's Miscellaneous Papers* (pp: 146-152), Macmillan and Co., London.
- [22] VanLandingham, M.R., Villarubia, J.S, Guthrie, W.F. and Meyers, G.F. (2001) Nanoindentation of polymers: An overview in recent advances in scanning probe microscopy. In: Tsukruk, V.V. and N.D. Spencer (Eds.), *Macromolecular Symposia* (pp. 83-88), Wiley-VCH Verlag GmbH & Co. KGaA, Weinheim.
- [23] Elmustafa, A.A. and Stone, D.S. (2003) Nanoindentation and the indentation size effect: Kinetics of deformation and strain gradient plasticity. *Journal of Mechanics and Physics of Solids* **51**: 357-381.
- [24] Rodríguez, R. and Gutierrez, I. (2003) Correlation between nanoindentation and tensile properties: Influence of the indentation size effect. *Materials Science and Engineering* **A361**: 377-384.
- [25] McElhaney, K.W., Vlassak, J.J. and Nix, W.D. (1998) Determination of indenter tip geometry and indentation experiments. *Journal of Materials Research* **13**(5): 1300-1306.
- [26] Kibbe A.H. (2000) Indentation of polymeric materials. In: Rowe, R.C., Sheskey, P.J. and P.J. Weller (Eds.), *Handbook of Pharmaceutical Excipients* (pp.204-210), Pharmaceutical Press, American Pharmacists Association, Washington.
- [27] Muller, H. G. (1973) *An introduction to food rheology*, William Heinemann Ltd., London.
- [28] Train, D. (1957) Transmission of forces through a powder mass during the process of pelleting. *Transaction of IChemE* **35**: 258-266.
- [29] Roberts, R.J. and Rowe, R.C. (1987) The compaction of pharmaceutical and other model materials – A pragmatic approach. *Chemical Engineering Science* **42**(4): 903-911.

**NOTATIONS**

$A_I$	projection of the contact area of the tip-material contact	(m <sup>2</sup> )
$B_o$	constant coefficient from the curve fitting of the contact area	(-)
$C_{if}$	calibration of the force compliance	(-)
$C_s$	material compliance	(-)
$C_{total}$	total compliance	(-)
$dh/dt$	drift rate	(m/s)
$E$	modulus of elasticity	(Pa)
$E_r$	reduced modulus	(Pa)
$E_I$	elastic modulus of the indenter	(Pa)
$h$	penetration depth	(m)
$h_c$	apparent material displacement	(m)
$h_{com}$	displacement of the die during compliance test	(m)
$h_f$	final displacement	(m)
$h_{if}$	displacement of the force frame	(m)
$h_s$	elastic displacement	(m)
$h_{max}$	maximum displacement of the indenter	(m)
$P$	force	(N)
$P_{max}$	maximum force	(N)
$S$	contact stiffness	(MPa)